Viral fusion protein transmembrane domain adopts β-strand structure to facilitate membrane topological changes for virus–cell fusion

Hongwei Yao[a], Michelle W. Lee[b], Alan J. Waring[c,d], Gerard C. L. Wong[b], and Mei Hong[a,1]

[a]Department of Chemistry, Massachusetts Institute of Technology, Cambridge, MA 02139; [b]Department of Bioengineering, California NanoScience Institute, University of California, Los Angeles, CA 90095; [c]Department of Physiology and Biophysics, University of California, Irvine, CA 92697; and [d]Department of Medicine, Harbor University of California Los Angeles Medical Center, LA BioMed, Torrance, CA 90502

Edited by Lukas K. Tamm, University of Virginia, Charlottesville, VA, and accepted by the Editorial Board July 27, 2015 (received for review January 22, 2015)

The C-terminal transmembrane domain (TMD) of viral fusion proteins such as HIV gp41 and influenza hemagglutinin (HA) is traditionally viewed as a passive α-helical anchor of the protein to the virus envelope during its merger with the cell membrane. The conformation, dynamics, and lipid interaction of these fusion protein TMDs have so far eluded high-resolution structure characterization because of their highly hydrophobic nature. Using magic-angle-spinning solid-state NMR spectroscopy, we show that the TMD of the parainfluenza virus 5 (PIV5) fusion protein adopts lipid-dependent conformations and interactions with the membrane and water. In phosphatidylcholine (PC) and phosphatidylglycerol (PG) membranes, the TMD is predominantly α-helical, but in phosphatidylethanolamine (PE) membranes, the TMD changes significantly to the β-strand conformation. Measured order parameters indicate that the strand segments are immobilized and thus oligomerized. ^{31}P NMR spectra and small-angle X-ray scattering (SAXS) data show that this β-strand–rich conformation converts the PE membrane to a bicontinuous cubic phase, which is rich in negative Gaussian curvature that is characteristic of hemifusion intermediates and fusion pores. ^{1}H-^{31}P 2D correlation spectra and ^{2}H spectra show that the PE membrane with or without the TMD is much less hydrated than PC and PG membranes, suggesting that the TMD works with the natural dehydration tendency of PE to facilitate membrane merger. These results suggest a new viral-fusion model in which the TMD actively promotes membrane topological changes during fusion using the β-strand as the fusogenic conformation.

solid-state NMR spectroscopy | small-angle X-ray scattering | conformational polymorphism | membrane curvature | peptide–membrane interactions

Viral fusion proteins mediate entry of enveloped viruses into cells by merging the viral lipid envelope and the cell membrane. The membrane-interacting subunit of these glycoproteins contains two hydrophobic domains: a fusion peptide (FP) that is usually located at the N terminus and a transmembrane domain (TMD) at the C terminus (1). Together, these domains sandwich a water-soluble ectodomain with a helical segment that trimerizes into a coiled coil. During virus–cell fusion, the trimeric protein, which initially adopts a compact structure, unfolds to an extended intermediate that exposes the FP to the target cell membrane while keeping the TMD in the virus envelope. This extended conformation then folds onto itself to form a trimer of hairpins, in so doing pulling the cell membrane and the virus envelope into close proximity (2, 3). Subsequently, the FP and TMD are hypothesized to deform the two membranes and dehydrate them (4), eventually causing a fusion pore and a fully merged membrane. In the postfusion state, most viral fusion proteins exhibit a six-helix-bundle structure in the ectodomain due to the trimer of hairpins (5).

This model of virus–cell fusion largely derives from crystal structures of fusion proteins in the pre- and postfusion states, most of which, however, do not contain the FP and TMD because of their hydrophobic nature. Thus, the mechanism of membrane deformation and dehydration, the potential mutual influence of this deformation and hairpin formation, and the high-resolution structures of the FP and TMD in the membrane have remained elusive. It is also unknown how FP and TMD help to lower the free energies of membrane formation and subsequent destruction of fusion intermediates such as the lipid stalk, which have been observed in protein-free membrane fusion (6).

Extensive spectroscopic studies have shown that influenza, HIV, and paramyxovirus FPs are conformationally plastic and adopt a partially inserted topology in the membrane to induce nonlamellar structures (7–11). In comparison, little is known about the structures of the C-terminal TMD of viral fusion proteins. Cysteine-scanning and sedimentation equilibrium data showed that various paramyxovirus TMDs form three-helix bundles in lipid membranes (12, 13). Circular dichroism (CD) and Fourier-transform infrared (FT-IR) data of influenza HA TMD indicate an α-helical structure parallel to the membrane normal (14). HIV gp41 gives broadened NMR signals for the TMD and its adjacent ectodomain residues in detergent micelles (15), indicating conformational exchange. Although most fusion models depict the TMDs as membrane-spanning α-helices, CD data of some viral and SNARE fusion protein TMDs reported β-strand conformation under certain conditions, and the strand structure may be correlated with the transition from hemifusion to fusion pore (16, 17). Despite these results, residue-specific structural information of viral fusion TMDs remains scarce, even though increasing biochemical evidence suggests that these TMDs

Significance

Enveloped viruses enter cells by fusing their lipid envelope with the cell membrane. The transmembrane domain (TMD) of viral fusion proteins is traditionally envisioned as a passive α-helical membrane anchor during the protein-mediated membrane fusion. Using solid-state NMR, we show that a parainfluenza virus fusion protein TMD exhibits lipid-dependent conformations. α-Helical structure dominates in phosphocholine and phosphoglycerol membranes, whereas β-strand conformation dominates in phosphoethanolamine membranes. Importantly, the β-strand–rich conformation quantitatively transforms the 1,2-dioleoyl-*sn*-glycero-3-phosphoethanolamine (DOPE) membrane to a bicontinuous cubic phase, which is rich in the saddle-splay curvature in hemifusion intermediates and fusion pores. Thus, viral fusion protein TMDs play an active role in virus entry by mediating the necessary membrane topological changes.

Author contributions: M.H. designed research; H.Y., M.W.L., A.J.W., G.C.L.W., and M.H. performed research; H.Y., M.W.L., A.J.W., G.C.L.W., and M.H. analyzed data; and H.Y., M.W.L., A.J.W., G.C.L.W., and M.H. wrote the paper.

The authors declare no conflict of interest.

This article is a PNAS Direct Submission. L.K.T. is a guest editor invited by the Editorial Board.

[1]To whom correspondence should be addressed. Email: meihong@mit.edu.

This article contains supporting information online at www.pnas.org/lookup/suppl/doi:10.1073/pnas.1501430112/-/DCSupplemental.

encode sequence-specific information for fusion. For example, replacing the TMDs of parainfluenza virus 5 (PIV5) and Newcastle disease virus fusion proteins with comparable domains of other paramyxovirus fusion proteins altered the ectodomain structure and reduced fusion, indicating site-specific interactions between the ectodomain and the TMD (18, 19). Various studies also suggested that the TMDs may modulate membrane curvature. For example, replacing the HA TMD by glycosylphosphatidylinositol, which inserts only into the outer leaflet of lipid membranes, arrested fusion at the hemifusion stage (20), and the block was released when positive-curvature molecules were added to the inner leaflet (21). Clearly, elucidating TMDs' roles in viral membrane fusion requires quantitative studies that simultaneously monitor how the TMD structure is influenced by lipids and how the TMD in turn impacts the curvature and hydration of membranes.

In this study, we investigate the structure and dynamics of the PIV5 TMD and correlate them with membrane structural changes. Parainfluenza viruses are the cause of infant respiratory diseases such as bronchiolitis and pneumonia (22). PIV5 enters cells using an attachment protein and the fusion protein F (23), which shares many common features with the HIV and influenza fusion proteins (1, 5). Thus, structure elucidation of the PIV5 TMD may give general insight into the mechanism of action of this class of viral fusion proteins. Using magic-angle–spinning (MAS) solid-state NMR spectroscopy, we show that the PIV5 TMD changes its conformation in response to the lipid composition and can adopt either α-helical or β-strand conformations. Importantly, ^{31}P and ^{2}H NMR data indicate that the TMD generates strong curvature and causes low hydration to phosphatidylethanolamine (PE)-rich membranes, in which the peptide has a β-strand–rich conformation. Synchrotron small-angle X-ray scattering (SAXS) data show that this β-strand–rich structure transforms the PE membrane to a bicontinuous cubic phase with negative Gaussian curvature (NGC), the type of curvature that underlies membrane scission and fusion. These results suggest that viral fusion TMDs actively facilitate the topological changes necessary for membrane restructuring during viral fusion.

Results

PIV5 TMD Changes Its Conformation in Response to the Membrane Composition. To determine the backbone conformation of the membrane-bound TMD, we measured ^{13}C and ^{15}N chemical shifts of residues distributed throughout the peptide. Cα, Cβ, C′, and ^{15}N chemical shifts are highly sensitive to backbone (ϕ, ψ) angles (24, 25). Because the PIV5 FP structure depends on the membrane environment, including the membrane surface charge, lipid chain unsaturation, and lipid intrinsic curvature (11, 26), we measured the TMD chemical shifts in six lipid membranes in the gel- and liquid-crystalline phases, to probe both the rigid-limit structure and the dynamics of the peptide. Two-dimensional ^{13}C-^{13}C correlation spectra of the TMD (Fig. 1 and *SI Appendix*, Fig. S1) bound to the neutral 1-palmitoyl-2-oleoyl-*sn*-glycero-3-phosphocholine (POPC) membrane show predominantly α-helical chemical shifts, but the C-terminal S505 and V506 also exhibit nonnegligible β-strand intensities. The deviations of the measured chemical shifts from the random-coil values (*SI Appendix*, Fig. S2) confirm the helical nature of the major conformer. At low temperature, the Cα-Cβ or Cα/β-CO cross-peak intensities indicate that the α-helical fraction is >93% for most residues but 75–85% for S505 and V506 (*SI Appendix*, Table S1). Compared with the FP in the same membrane, the TMD is more α-helical. Interestingly, the I488 Cα-Cβ peak has lower intensity than the other residues (*SI Appendix*, Table S2), indicating that the N terminus is more disordered than the rest of the peptide. Alanine mutagenesis of the TMD (12) found L486 and I488 to be crucial for membrane fusion; thus, this conformational disorder may be functionally relevant.

To investigate if negatively charged lipids and cholesterol affect the TMD conformation, we measured 2D ^{13}C-^{13}C and ^{15}N-^{13}C correlation spectra of TMD in the POPC/1-palmitoyl-2-oleoyl-*sn*-glycero-3-phosphatidylglycerol (POPG) and POPC/cholesterol

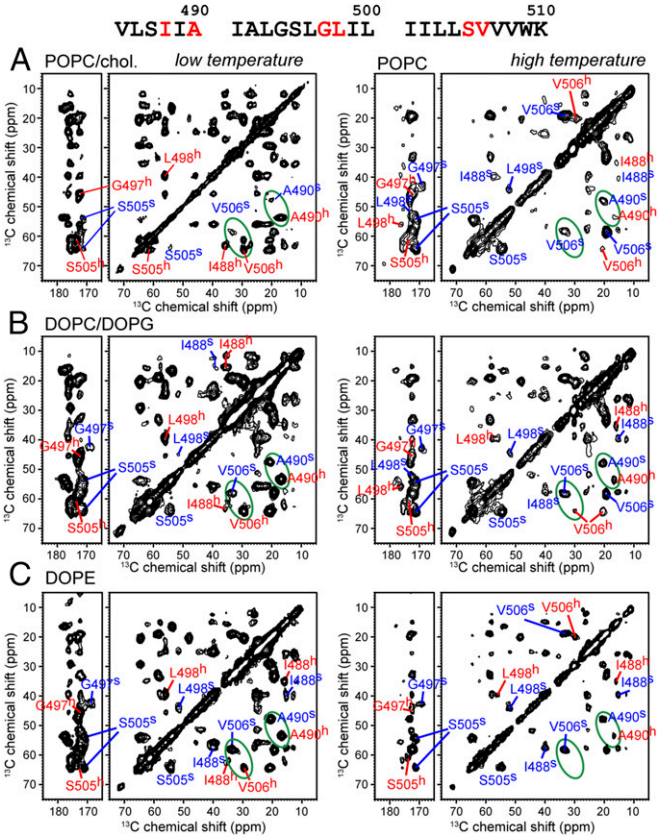

Fig. 1. Two-dimensional ^{13}C-^{13}C correlation spectra of the PIV5 TMD in POPC/cholesterol (*Left*) and POPC (*Right*) (*A*), DOPC/DOPG (*B*), and DOPE membranes (*C*). (*A*–*C*) Low-temperature spectra (243–253 K) (*Left*) allow quantification of the helix and strand intensities, whereas high-temperature spectra (293–303 K) (*Right*) report the peptide mobility in liquid-crystalline membranes. α-Helix signals (red) dominate in *A* and *B*, whereas β-strand signals (blue) become significant in the PE membrane. Superscripts "h" and "s" denote helix and strand, respectively, and ovals highlight the A490 and V506 peaks.

membranes (Figs. 1 and 2 and *SI Appendix*, Fig. S1). The spectra indicate that the α-helical content of the TMD is unaffected by POPG and cholesterol, and the C terminus retains the slightly higher β-strand content. In comparison, increased chain unsaturation in the 1,2-dioleoyl-*sn*-glycero-3-phosphocholine (DOPC)/1,2-dioleoyl-*sn*-glycero-3-phosphatidyl-glycerol (DOPG) membrane noticeably increased the β-strand intensities of the N- and C-terminal residues, whereas the central residues, G497 and L498, remain predominantly helical. The average α-helical content of the peptide decreased to 80%, compared with 91–95% for the POPC and POPC/POPG samples. Thus, higher lipid-chain disorder, with the concomitant increase in the negative membrane curvature, shifts the TMD conformational equilibrium to β-strand. This trend is identical to the response of the FP to lipid unsaturation (11).

To further examine the effects of negative membrane curvature on the TMD structure, we measured the 2D spectra of TMD in 1-palmitoyl-2-oleoyl-*sn*-glycero-3-phosphoethanolamine (POPE) and 1,2-dioleoyl-*sn*-glycero-3-phosphoethanolamine (DOPE) membranes. The spectra (Figs. 1 and 2 and *SI Appendix*, Fig. S1) show a significant increase of β-strand intensities, which now account for 61% and 42% of the total intensities of the POPE- and DOPE-bound peptides, respectively (Fig. 2*D*). This β-strand conformation was stabilized after several days, whereas the initial structure was more helical (*SI Appendix*, Fig. S3).

In the liquid-crystalline phase of all membranes, the α-helical signals are significantly suppressed but the β-strand peaks remain,

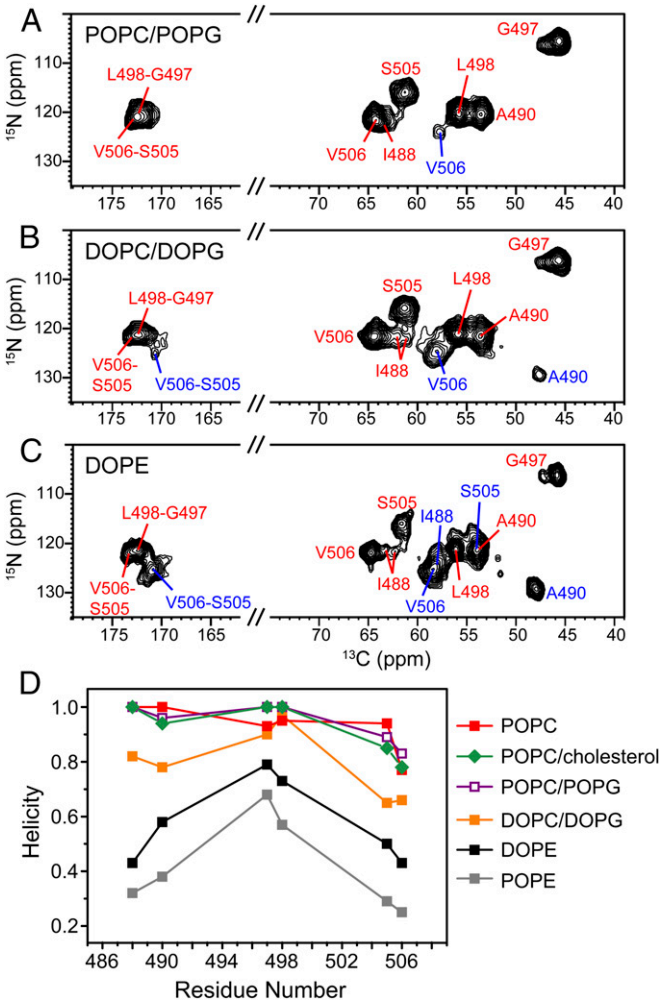

Fig. 2. (*A*–*C*) Low-temperature 2D ^{15}N-^{13}C correlation spectra of the TMD bound to POPC/POPG (*A*), DOPC/DOPG (*B*), and DOPE membranes (*C*). The TMD is mainly α-helical in the POPC/POPG membrane but becomes more β-strand in the DOPE membrane, consistent with the 2D ^{13}C-^{13}C spectra. (*D*) Residue-specific helix fractions of membrane-bound TMD obtained from Cα-Cβ or Cα/β-CO cross-peak intensities. The TMD is mostly helical in PC and PG membranes but switches to the strand conformation in PE membranes.

indicating that the helical segments undergo intermediate-timescale motion, whereas the β-strand domains are immobilized by oligomerization. In the POPE membrane, site-specific C-H dipolar couplings indicate bond order parameters of 0.84–0.93 for the β-strand residues (*SI Appendix*, Fig. S4), confirming that only small-amplitude local motions exist in the β-strands.

Taken together, these results indicate that (*i*) negative-curvature PE lipids are the main conformational switches of the TMD; (*ii*) the central portion of the TMD is the α-helical core whereas the two termini have higher β-strand propensities; and (*iii*) the N terminus is more disordered than the rest of the peptide. All labeled residues exhibit the same set of helical and strand chemical shifts in various membranes (*SI Appendix*, Table S3), and only their relative intensities change; thus, the conformational distribution is bimodal. CD spectra indicate that the TMD conformation is similar between peptide/lipid molar ratios of 1/100 and 1/20 (*SI Appendix*, Fig. S5 and Table S4). This concentration independence, combined with the fact that the central segment remains mostly helical in all membranes, and the peptide is well inserted into the membranes (see *The TMD Inserts into Lipid Membranes*), indicates that the terminal strand conformations are not due to nonspecific aggregation but are intrinsic to the amino acid sequence and the membrane used. Because the CD spectra were measured at ambient temperature, they also imply that the α-helical residues, although undetectable in the high-temperature NMR spectra because of motion, remain helical in the liquid-crystalline membrane.

The TMD Inserts into Lipid Membranes. To determine whether the PIV5 TMD inserts into the hydrophobic part of the membrane, we measured lipid–peptide ^{1}H-^{13}C 2D correlation spectra with ^{1}H spin diffusion. In liquid-crystalline POPE, cross-peaks of lipid-chain protons with both β-strand and α-helical ^{13}C signals are observed (Fig. 3), and the cross-peak intensities as a function of mixing time are well fit to a distance of ∼2 Å using previously calibrated diffusion coefficients (27). Thus, the peptide spans the POPE membrane, in close contact with the methylene groups. ^{1}H-^{13}C correlation spectra were also measured in gel-phase POPC/POPG membrane (28) for the immobilized α-helical peptide, and the spectra indicate a similar membrane-spanning topology, with lipid–peptide cross-peaks dominating water-peptide cross-peaks (*SI Appendix*, Fig. S6). Thus, both helical and mixed-conformation peptides are well inserted into the membrane.

The TMD Causes Negative Gaussian Curvature and Low Hydration to PE Membranes. We used static ^{31}P and ^{2}H NMR to probe the membrane curvature and dynamics upon peptide binding. The POPC and POPC/POPG membranes exhibit uniaxial ^{31}P line shapes in the absence and presence of the peptide (Fig. 4*A*), indicating that the lamellar structure of the bilayers is unperturbed by the α-helical TMD. For DOPC/DOPG and POPE membranes, the TMD caused an additional isotropic peak, indicating the onset of membrane curvature as the β-strand content increased. ^{2}H NMR spectrum of d_{31}-POPE also exhibits an isotropic peak (*SI Appendix*, Fig. S7), confirming that the isotropic ^{31}P peak results from membrane curvature rather than accidental magic-angle orientation of the lipid head group.

The most striking effect of the TMD on lipid membranes is observed for DOPE. Pure DOPE exhibits a lamellar-to-inverted-hexagonal (H_{II}) phase transition at ∼283 K, as shown by the characteristic ^{31}P NMR line shapes (Fig. 4*B*). TMD quantitatively converted both line shapes to an isotropic peak between 273 and 303 K. At 303 K, this isotropic peak accounts for 85% of the spectral intensity, whereas the H_{II} phase represents 15%. Thus, the TMD increased the transition temperature by more than 20 K.

The isotropic ^{31}P chemical shift could result from isotropic micelles, small vesicles, or bicontinuous cubic phases (29). Because the long-chain DOPE is unlikely to form micelles, we suspected that the membrane may be transformed to a cubic phase. To determine the membrane morphology directly, we measured the SAXS spectra of TMD-bound DOPE (Fig. 5). Two sets of correlation peaks were observed. The first set has Q ratios of $\sqrt{6}$: $\sqrt{8}$: $\sqrt{20}$: $\sqrt{22}$: $\sqrt{50}$: $\sqrt{54}$, which indexes to an Ia3d gyroid phase (30) with a lattice parameter a of 12.0 nm. The second set shows Q ratios of $\sqrt{2}$: $\sqrt{3}$: $\sqrt{4}$: $\sqrt{7}$: $\sqrt{9}$: $\sqrt{12}$: $\sqrt{13}$, which indexes to an H_{II} phase with $a = 5.8$ nm. As a bicontinuous cubic phase, Ia3d has two nonintersecting water channels separated by a lipid bilayer (31). The center of this bilayer traces a minimal surface whose principal curvatures, c_1 and c_2, are equal and opposite in sign at every point, so that this minimal surface has zero mean curvature and negative Gaussian curvature, $K = c_1 \cdot c_2 < 0$. NGC of bilayer membranes has also been observed in the scission necks of budding vesicles and fusion pores. For a bicontinuous cubic phase, the average NGC, $\langle K \rangle$, is a quantitative measure of the amount of NGC induced in the membrane and depends on the lattice parameter as $\langle K \rangle = 2\pi\chi/A_0a^2$, where the Euler characteristic χ and the surface area per unit cell A_0 are constants of the phase (31, 32). For $a = 12.0$ nm, the average NGC is $\langle K \rangle = -0.112$ nm^{-2}.

Because membrane fusion requires transient dehydration of the contacting surfaces of the two membranes, we tested the effects of the PIV5 TMD on membrane hydration using 2D ^{1}H-^{31}P correlation (33) and ^{2}H NMR experiments. Well-

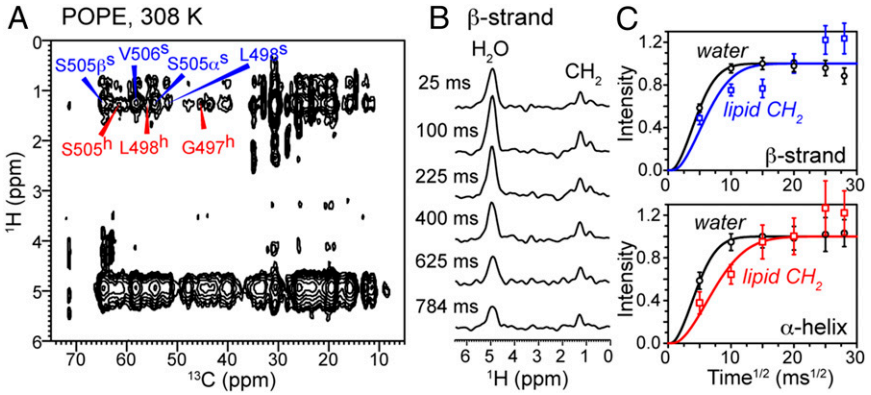

Fig. 3. Two-dimensional ^{1}H-^{13}C correlation spectra of POPE-bound TMD. (*A*) Two-dimensional spectrum with a 100-ms ^{1}H spin-diffusion mixing time. (*B*) ^{1}H cross-sections of the sum of β-strand signals as a function of mixing time. (*C*) Water–peptide (black) and lipid–peptide polarization transfer curves for the β-strand (blue) and α-helical (red) signals. The fast buildup indicates that both helical and strand conformations are well inserted into the membrane.

resolved water–^{31}P cross-peaks are observed for the phosphatidylcholine (PC) and phosphatidylglycerol (PG) membranes, but the water cross-peak is much weaker and broader for POPE with or without the peptide (Fig. 4 *C*–*E*), indicating low hydration. ^{2}H NMR spectra of D_2O bound to POPE membranes without and with the TMD at similar water contents (34, 35) show a superposition of a quadrupolar splitting, which results from tightly bound water, and an isotropic peak, which results from free water (*SI Appendix*, Fig. S7*C*). Importantly, the TMD-containing POPE exhibits higher isotropic intensity and larger quadrupolar coupling than the pure POPE membrane, indicating that the TMD moderately increases the dehydration tendency of the POPE membrane by diverting water from the membrane surface.

Discussion

To our knowledge, these solid-state NMR and SAXS data provide the first structural evidence that a viral fusion TMD causes significant membrane curvature, especially to PE membranes, and the β-strand conformation correlates with this curvature generation. Compared with the FP of the same protein, which converted only a small fraction of the DOPE ^{31}P spectrum to an isotropic peak (11), the TMD converted most of the intensity to an isotropic peak, indicating that the TMD has stronger curvature-generating ability than the FP. These results counter the prevailing view that viral fusion TMDs are a passive membrane anchor while the FPs are the chief causative agent of bilayer destabilization (36–38).

The type of curvature generated by the PIV5 TMD is NGC, as revealed by the SAXS data. NGC is geometrically necessary for topological changes during membrane remodeling in biological processes such as virus budding and membrane scission (39, 40). NGC generation is often facilitated by negative-curvature lipids such as PE (41–43), which commonly enhance fusogenicity (44). Our measured $\langle K \rangle$ can be visualized using a catenoid surface, which is an approximation of a scission neck or a fusion pore (45, 46). The Gaussian curvature of a minimal catenoid surface with a neck radius of c along its z axis is $K(z) = -[sech^4(z/c)]/c^2$. The $\langle K \rangle$ value of -0.112 nm^{-2} for the TMD-induced Ia3d phase corresponds to a catenoid hemifusion stalk with a ∼6 nm width at the narrowest cross-section (Fig. 5*C*), which is ∼30-fold smaller than the PIV5 virus diameter of 150–200 nm (47). Adding the bilayer thickness, this neck diameter translates to a hemifusion-stalk waist of ∼10 nm, which is in excellent agreement with the estimated waist of ∼9 nm for a pure-DOPE stalk (48). This suggests that the TMD works with the natural structural tendencies of PE to stabilize the fusion intermediate. Although proteins clearly play a key role in fusion, membrane merger can also be strongly influenced by the constituent lipids. The tendency of the leaflets to bend in specific directions dictates the energy of a fusion intermediate such as a hemifusion stalk. Our data suggest that PE-rich regions of the viral membrane are especially susceptible to TMD-induced bending and dehydration and thus may play a central role in the fusion process.

Which structural features of the TMD are responsible for imparting the NGC to PE membranes? ^{13}C and ^{15}N chemical shifts indicate that the two termini of the peptide have high β-strand propensities, whereas the center is more helical, suggesting that this strand–helix–strand motif may endow the TMD with the ability to perturb the two membrane leaflets differently to generate NGC. The 26-residue peptide is sufficient to span the membrane: as a pure α-helix, it would be ∼39 Å long, and the β-strand residues further increase the peptide length, making it possible for the TMD to tilt, bend, and acquire local disorder while still spanning the membrane. This strand–helix–strand conformation may be particularly effective in generating membrane curvature, because β-strands are inherently anisotropic and can have different surface normal orientations (Fig. 6). Such orientational differences, together with the higher N-terminal disorder, may impact lipid packing near the hydrophilic surfaces of the two leaflets differently, thus creating the orthogonal curvatures necessary for NGC. Previous work has shown that structural perturbations near the hydrophobic/hydrophilic interface of the membrane have particularly large effects on lipid packing, membrane curvature, and phase behavior (49). We hypothesize that the NGC induced in PE membranes may play an important role in stabilizing the necessary curvature of the hemifusion stalks in the outer leaflets, which have more complex lipid compositions (50).

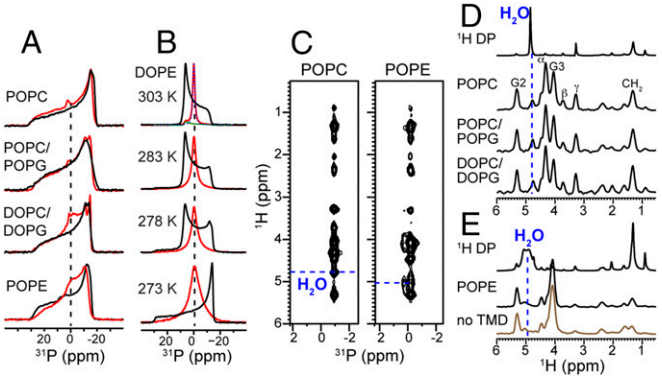

Fig. 4. Effects of the TMD on membrane curvature and hydration. (*A*) Static ^{31}P spectra of POPC, POPC/POPG, DOPC/DOPG, and POPE membranes without (black) and with (red) the TMD. (*B*) Static ^{31}P spectra of DOPE without and with the TMD from 273 K to 303 K. The TMD converted the lamellar and H_{II} powder patterns to an isotropic peak. Deconvolution of the 303 K spectrum shows that ∼15% of the intensity remained in the H_{II} phase (green). (*C*) Two-dimensional MAS ^{1}H-^{31}P correlation spectra of POPC and POPE membranes with 100-ms ^{1}H spin diffusion. (*D* and *E*) ^{1}H cross-sections of the 2D ^{1}H-^{31}P spectra. (*D*) The PC and PG membranes exhibit a strong water cross-peak. (*E*) POPE membranes with (black) and without (brown) the TMD show a broad water cross-peak, indicating low hydration.

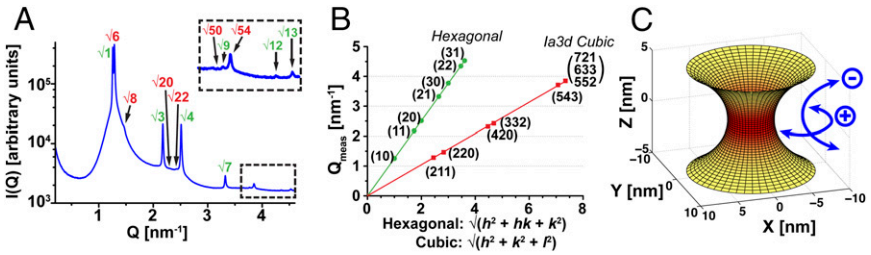

Fig. 5. The TMD generates NGC to the DOPE membrane. (*A*) SAXS spectrum of TMD-bound DOPE. An Ia3d cubic phase (red) coexists with an H_{II} phase (green). (*Inset*) An expanded view of the higher order reflections. (*B*) Measured *Q* positions versus assigned reflections in terms of Miller indices *h*, *k*, and *l*. Q_{meas} is plotted versus $(h^2+k^2+l^2)$ for the cubic phase and (h^2+hk+k^2) for the H_{II} phase. (*C*) A catenoid surface with a 6-nm diameter (c = 3 nm) has K = −0.111 nm^{-2} at its narrowest cross-section. A hemifusion stalk or fusion pore will have a neck that conforms to the catenoid. Arrows indicate directions of negative and positive principal curvatures.

In addition to promoting NGC, a β-strand–rich conformation may also facilitate fusion by forming trimeric sheets and clustering multiple trimers at the fusion site. The observed immobilization of the β-strand residues in the high-temperature spectra and the high-order parameters strongly suggest that the β-strands are oligomerized into β-sheets, because monomeric peptides or very small oligomers should undergo fast uniaxial rotation in lipid membranes (51). In principle, the strand–helix–strand peptide can pack in a parallel or antiparallel fashion. Preliminary 2D ^{13}C correlation spectra measured with long mixing times show no cross-peaks between the N- and C-terminal residues (*SI Appendix*, Fig. S8), suggesting that antiparallel arrangement is unlikely but parallel packing is possible. Consistently, FT-IR spectrum of POPE-bound TMD shows an amide I peak at 1628 cm^{-1}, characteristic of β-sheet structures, but no peak at 1690 cm^{-1}, which is expected for antiparallel β-sheets, is detected (*SI Appendix*, Fig. S9). The exact oligomeric structure of PE-bound TMD requires intermolecular distance measurements. β-Strand peptides that form parallel transmembrane β-barrels have been observed in antimicrobial peptides (52), illustrating how backbone N-H and C=O hydrogen-bonds can lower the free energy cost of inserting the β-strands into the membrane.

Fig. 6 shows the proposed structural model of the TMD in PE membranes, taking into account the measured peptide conformation and topology, the inferred oligomeric packing, and the observed membrane curvature. Although the exact oligomeric structure requires experimental distance constraints, a first evaluation of the model is provided by molecular dynamics simulations (*SI Appendix*, Fig. S10), which show that a parallel homotrimer of the strand–helix–strand TMD can be stabilized in the POPE membrane for 90 ns. The energetic cost of burying in the membrane disordered residues between the strands and helix may be offset by the oligomerization of the peptide, the natural conformational tendency of the two Gly residues in the potential helix–strand transition region, membrane thinning, and other defects.

Although the lipid composition has an enormous impact on the TMD conformation, the amino acid sequence of the TMD also encodes an inherent preference for β-strands. Out of 26 residues, the PIV5 TMD contains 10 β-branched residues Val and Ile (*SI Appendix*, Table S5), which are known to destabilize α-helices. High Val and Ile contents in synthetic LV peptides and other viral TMDs have been shown to cause higher fusogenicity, possibly by increasing conformational flexibility and reducing the α-helical content (12, 13, 53, 54). Indeed, β-branched residues constitute 30–75% of the TMD sequences of 10 paramyxoviruses and HIV, suggesting that transition to the β-strand conformation in PE-rich membranes may be general for this class of fusion proteins.

Although both the FP and TMD of PIV5 exhibit lipid-induced conformational changes, and both peptides adopt β-strand–rich structures in PE membranes, subtle structural features differ. The TMD is mostly α-helical in both neutral and anionic membranes, and PE is the main trigger for the switch to the β-strand conformation. In comparison, the FP is entirely β-strand in PC and PE membranes and converts to the helical conformation by anionic lipids (11, 26). The distinct lipid dependences of FP and TMD structures may enable the intact protein to adapt to different lipid environments of the virus envelope and cell membrane (50).

In PE and other membranes with negative spontaneous curvature, the N terminus of the FP has the highest β-strand propensity (11), whereas the C terminus of the TMD forms the most-ordered β-strand. Thus, if the FP and TMD reside in the same region that is rich in PE, their β-strands may associate. This state may occur at the end of the ectodomain hairpin formation, when the membrane transitions from the hemifusion state to the fusion pore. Future experiments measuring the quaternary structure of the FP and TMD will be important to elucidate the structural basis for the hemifusion-to-fusion-pore transition. Taken together, the present data suggest a viral fusion model that departs significantly from the helix-centric models so far, by showing that the TMD of this viral fusion protein uses the β-strand conformation to achieve the necessary curvature and low hydration for membrane fusion.

Methods

Isotopically labeled TMD of PIV5 F was chemically synthesized and purified by HPLC. The peptide was bound to six different lipid membranes for NMR experiments at 600-, 400-, and 900-MHz ^1H Larmor frequencies. Additional experimental details are provided in the *SI Appendix*.

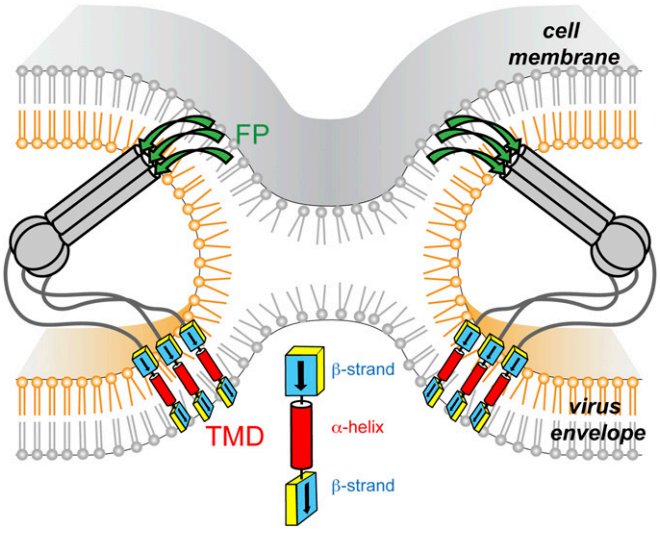

Fig. 6. Structural model of TMD in PE-rich membranes. The TMD adopts a transmembrane strand–helix–strand conformation, which imparts different curvatures to the two leaflets of the membrane. The β-strand segments are immobilized by oligomerization. In these PE-rich membranes, previous data showed that the FP (green) is also rich in β-strand conformation.

ACKNOWLEDGMENTS. This work is supported by National Institutes of Health (NIH) Grant GM066976 (to M.H.) and National Science Foundation (NSF) Grants DMR1106106 and DMR1411329 (to G.C.L.W.). The 900-MHz spectra were measured at the Massachusetts Institute of Technology/Harvard Center for Magnetic Resonance, which is supported by NIH Grant EB002026.

1. Lamb RA, Jardetzky TS (2007) Structural basis of viral invasion: Lessons from paramyxovirus F. *Curr Opin Struct Biol* 17(4):427–436.
2. Harrison SC (2008) Viral membrane fusion. *Nat Struct Mol Biol* 15(7):690–698.
3. Eckert DM, Kim PS (2001) Mechanisms of viral membrane fusion and its inhibition. *Annu Rev Biochem* 70:777–810.
4. Tamm LK (2003) Hypothesis: Spring-loaded boomerang mechanism of influenza hemagglutinin-mediated membrane fusion. *Biochim Biophys Acta* 1614(1):14–23.
5. White JM, Delos SE, Brecher M, Schornberg K (2008) Structures and mechanisms of viral membrane fusion proteins: Multiple variations on a common theme. *Crit Rev Biochem Mol Biol* 43(3):189–219.
6. Chernomordik LV, Kozlov MM (2008) Mechanics of membrane fusion. *Nat Struct Mol Biol* 15(7):675–683.
7. Tamm LK, Crane J, Kiessling V (2003) Membrane fusion: A structural perspective on the interplay of lipids and proteins. *Curr Opin Struct Biol* 13(4):453–466.
8. Qiang W, Sun Y, Weliky DP (2009) A strong correlation between fusogenicity and membrane insertion depth of the HIV fusion peptide. *Proc Natl Acad Sci USA* 106(36):15314–15319.
9. Lai AL, Moorthy AE, Li Y, Tamm LK (2012) Fusion activity of HIV gp41 fusion domain is related to its secondary structure and depth of membrane insertion in a cholesterol-dependent fashion. *J Mol Biol* 418(1-2):3–15.
10. Lorieau JL, Louis JM, Bax A (2010) The complete influenza hemagglutinin fusion domain adopts a tight helical hairpin arrangement at the lipid:water interface. *Proc Natl Acad Sci USA* 107(25):11341–11346.
11. Yao H, Hong M (2014) Conformation and lipid interaction of the fusion peptide of the paramyxovirus PIV5 in anionic and negative-curvature membranes from solid-state NMR. *J Am Chem Soc* 136(6):2611–2624.
12. Bissonnette ML, Donald JE, DeGrado WF, Jardetzky TS, Lamb RA (2009) Functional analysis of the transmembrane domain in paramyxovirus F protein-mediated membrane fusion. *J Mol Biol* 386(1):14–36.
13. Smith EC, et al. (2012) Beyond anchoring: The expanding role of the hendra virus fusion protein transmembrane domain in protein folding, stability, and function. *J Virol* 86(6):3003–3013.
14. Tatulian SA, Tamm LK (2000) Secondary structure, orientation, oligomerization, and lipid interactions of the transmembrane domain of influenza hemagglutinin. *Biochemistry* 39(3):496–507.
15. Lakomek NA, et al. (2013) Internal dynamics of the homotrimeric HIV-1 viral coat protein gp41 on multiple time scales. *Angew Chem Int Ed Engl* 52(14):3911–3915.
16. Dennison SM, Greenfield N, Lenard J, Lentz BR (2002) VSV transmembrane domain (TMD) peptide promotes PEG-mediated fusion of liposomes in a conformationally sensitive fashion. *Biochemistry* 41(50):14925–14934.
17. Langosch D, et al. (2001) Peptide mimics of SNARE transmembrane segments drive membrane fusion depending on their conformational plasticity. *J Mol Biol* 311(4):709–721.
18. Gravel KA, McGinnes LW, Reitter J, Morrison TG (2011) The transmembrane domain sequence affects the structure and function of the Newcastle disease virus fusion protein. *J Virol* 85(7):3486–3497.
19. Zokarkar A, Lamb RA (2012) The paramyxovirus fusion protein C-terminal region: Mutagenesis indicates an indivisible protein unit. *J Virol* 86(5):2600–2609.
20. Kemble GW, Danieli T, White JM (1994) Lipid-anchored influenza hemagglutinin promotes hemifusion, not complete fusion. *Cell* 76(2):383–391.
21. Melikyan GB, Brener SA, Ok DC, Cohen FS (1997) Inner but not outer membrane leaflets control the transition from glycosylphosphatidylinositol-anchored influenza hemagglutinin-induced hemifusion to full fusion. *J Cell Biol* 136(5):995–1005.
22. Chang A, Dutch RE (2012) Paramyxovirus fusion and entry: Multiple paths to a common end. *Viruses* 4(4):613–636.
23. Jardetzky TS, Lamb RA (2014) Activation of paramyxovirus membrane fusion and virus entry. *Curr Opin Virol* 5:24–33.
24. de Dios AC, Pearson JG, Oldfield E (1993) Secondary and tertiary structural effects on protein NMR chemical shifts: An ab initio approach. *Science* 260(5113):1491–1496.
25. Shen Y, et al. (2008) Consistent blind protein structure generation from NMR chemical shift data. *Proc Natl Acad Sci USA* 105(12):4685–4690.
26. Yao H, Hong M (2013) Membrane-dependent conformation, dynamics, and lipid interactions of the fusion peptide of the paramyxovirus PIV5 from solid-state NMR. *J Mol Biol* 425(3):563–576.
27. Huster D, Yao X, Hong M (2002) Membrane protein topology probed by (1)H spin diffusion from lipids using solid-state NMR spectroscopy. *J Am Chem Soc* 124(5):874–883.
28. Wang T, Yao H, Hong M (2013) Determining the depth of insertion of dynamically invisible membrane peptides by gel-phase ^{1}H spin diffusion heteronuclear correlation NMR. *J Biomol NMR* 56(2):139–148.
29. Yang Y, Yao H, Hong M (2015) Distinguishing bicontinuous lipid cubic phases from isotropic membrane morphologies using (31)P solid-state NMR spectroscopy. *J Phys Chem B* 119(15):4993–5001.
30. Squires AM, et al. (2002) Kinetics and mechanism of the lamellar to gyroid inverse bicontinuous cubic phase transition. *Langmuir* 18:7384–7392.
31. Shearman GC, Ces O, Templer RH, Seddon JM (2006) Inverse lyotropic phases of lipids and membrane curvature. *J Phys Condens Matter* 18(28):S1105–S1124.
32. Siegel DP (2010) Fourth-order curvature energy model for the stability of bicontinuous inverted cubic phases in amphiphile-water systems. *Langmuir* 26(11):8673–8683.
33. Williams JK, Hong M (2014) Probing membrane protein structure using water polarization transfer solid-state NMR. *J Magn Reson* 247:118–127.
34. Gawrisch K, et al. (1992) Energetics of a hexagonal-lamellar-hexagonal-phase transition sequence in dioleoylphosphatidylethanolamine membranes. *Biochemistry* 31(11):2856–2864.
35. Marinov R, Dufourc EJ (1996) Thermotropism and hydration properties of POPE and POPE cholesterol systems as revealed by solid state H-2 and P-31-NMR. *Eur Biophys J* 24:423–431.
36. Tenchov BG, MacDonald RC, Lentz BR (2013) Fusion peptides promote formation of bilayer cubic phases in lipid dispersions. An x-ray diffraction study. *Biophys J* 104(5):1029–1037.
37. Colotto A, Epand RM (1997) Structural study of the relationship between the rate of membrane fusion and the ability of the fusion peptide of influenza virus to perturb bilayers. *Biochemistry* 36(25):7644–7651.
38. Pereira FB, Valpuesta JM, Basañez G, Goñi FM, Nieva JL (1999) Interbilayer lipid mixing induced by the human immunodeficiency virus type-1 fusion peptide on large unilamellar vesicles: The nature of the nonlamellar intermediates. *Chem Phys Lipids* 103(1-2):11–20.
39. Schmidt NW, et al. (2012) Molecular basis for nanoscopic membrane curvature generation from quantum mechanical models and synthetic transporter sequences. *J Am Chem Soc* 134(46):19207–19216.
40. Schmidt NW, et al. (2011) Criterion for amino acid composition of defensins and antimicrobial peptides based on geometry of membrane destabilization. *J Am Chem Soc* 133(17):6720–6727.
41. Zimmerberg J, Kozlov MM (2006) How proteins produce cellular membrane curvature. *Nat Rev Mol Cell Biol* 7(1):9–19.
42. Siegel DP, Kozlov MM (2004) The gaussian curvature elastic modulus of N-monomethylated dioleoylphosphatidylethanolamine: Relevance to membrane fusion and lipid phase behavior. *Biophys J* 87(1):366–374.
43. Leermakers FA (2013) Bending rigidities of surfactant bilayers using self-consistent field theory. *J Chem Phys* 138(15):154109.
44. Epand RM (1998) Lipid polymorphism and protein-lipid interactions. *Biochim Biophys Acta* 1376:353–368.
45. Boucrot E, et al. (2012) Membrane fission is promoted by insertion of amphipathic helices and is restricted by crescent BAR domains. *Cell* 149(1):124–136.
46. Schmidt NW, Mishra A, Wang J, DeGrado WF, Wong GC (2013) Influenza virus A M2 protein generates negative Gaussian membrane curvature necessary for budding and scission. *J Am Chem Soc* 135(37):13710–13719.
47. Terrier O, et al. (2009) Parainfluenza virus type 5 (PIV-5) morphology revealed by cryo-electron microscopy. *Virus Res* 142(1-2):200–203.
48. Siegel DP (1999) The modified stalk mechanism of lamellar/inverted phase transitions and its implications for membrane fusion. *Biophys J* 76(1 Pt 1):291–313.
49. Lewis RN, McElhaney RN, Harper PE, Turner DC, Gruner SM (1994) Studies of the thermotropic phase behavior of phosphatidylcholines containing 2-alkyl substituted fatty acyl chains: A new class of phosphatidylcholines forming inverted nonlamellar phases. *Biophys J* 66(4):1088–1103.
50. Gerl MJ, et al. (2012) Quantitative analysis of the lipidomes of the influenza virus envelope and MDCK cell apical membrane. *J Cell Biol* 196(2):213–221.
51. Cady SD, Goodman C, Tatko CD, DeGrado WF, Hong M (2007) Determining the orientation of uniaxially rotating membrane proteins using unoriented samples: A 2H, 13C, AND 15N solid-state NMR investigation of the dynamics and orientation of a transmembrane helical bundle. *J Am Chem Soc* 129(17):5719–5729.
52. Mani R, et al. (2006) Membrane-dependent oligomeric structure and pore formation of a beta-hairpin antimicrobial peptide in lipid bilayers from solid-state NMR. *Proc Natl Acad Sci USA* 103(44):16242–16247.
53. Hofmann MW, et al. (2004) De novo design of conformationally flexible transmembrane peptides driving membrane fusion. *Proc Natl Acad Sci USA* 101(41):14776–14781.
54. Poschner BC, Fischer K, Herrmann JR, Hofmann MW, Langosch D (2010) Structural features of fusogenic model transmembrane domains that differentially regulate inner and outer leaflet mixing in membrane fusion. *Mol Membr Biol* 27(1):1–10.